Nanoscale Advances

ROYAL SOCIETY OF CHEMISTRY

PAPER

View Article Online
View Journal | View Issue

Cite this: *Nanoscale Adv.*, 2025, **7**, 3375

Green synthesis of silver nanoparticles using the BT5 tea cultivar of Bangladesh: unveiling molecular mechanisms of anti-cancer activity in mice model†

Sk. Md. Atiqur Rahman,[abef] Rokshana Ara Ruhi,[abef] Md. Mahmudul Hasan Maruf,[b] Md. Ragib Shariar,[b] Mobasshir Noor Shehab,[b] Khaled Mahmud Sujon,[b] Mohammad Saiful Islam,[b] Md. Abdul Aziz,[c] Firoz Ahmed,[d] Ananda Kumar Saha,[f] Md. Anwarul Kabir Bhuiya*[e] and Md. Abu Reza*[b]

Silver nanoparticles (AgNPs) have sparked widespread interest due to their remarkable physiochemical capabilities, and they are now being used as a beneficial tool in the biomedical field. However, typical synthesis processes generate dangerous compounds that raise environmental and safety concerns. This is one of the main reasons for choosing a greener synthesis approach. The BT5 cultivar of green tea, which is high in phenolic and flavonoid compounds and has strong antioxidant activity ($IC_{50} \approx 97.8$ μg mL^{-1}), was used in an eco-friendly way to produce AgNPs. The green synthesis approach was confirmed by the rapid color change (light to dark brown) of $AgNO_3$ solution upon the addition of the BT5 extract. Several methods were performed to characterize the synthesized BT5-AgNPs, using UV-vis spectroscopy ($\lambda_{max} = 424$ nm), FTIR, DLS, zeta potential (-39.8 ± 0.45 mV), TGA, XRD (crystalline size = 11.25 nm), and FE-SEM (35 ± 8.36 nm). BT5-AgNPs showed strong antiproliferative properties inimical to Ehrlich-Lettre ascites carcinoma cells (EAC) of the Swiss albino variety of mice model, with low-concentration treatment (1 mg kg^{-1}) resulting in 52.15% cell growth inhibition. Fluorescence microscopy using DAPI staining revealed morphological alterations *via* heterochromatization and karyorrhexis. Gene expression analysis revealed upregulation of hallmark genes p53 and BAX and Bcl2 downregulation in the low- and high-concentration groups, indicating activation of the apoptotic pathway. Most likely due to cytotoxic effects and altered cellular responses, a higher dosage (5 mg kg^{-1}) resulted in slightly lower efficacy.

Received 3rd February 2025
Accepted 25th March 2025

DOI: 10.1039/d5na00115c

rsc.li/nanoscale-advances

Introduction

The use of nanoparticles is increasing exponentially worldwide because of their versatile use in industry, technology, and medicine. Their unique properties, including their greater surface-to-volume ratio, greater surface energy, and specific mechanical, thermal, electrical, magnetic, and optical characteristics, make them versatile for a wide range of applications and have enormous potential.[1] They can be created through various techniques, primarily categorized into top-down approaches, which involve breaking down larger materials, and bottom-up methods, where nanoparticles are synthesized from atomic precursors. Synthesis techniques can also be categorized based on the methodology employed: physical, chemical, or biological.[2] Although physiochemical reactions are the most efficient methods for nanoparticle synthesis, several other techniques like thermal, radiation/sono chemical, microwave-assisted, chemical reduction, and electrochemical processes are also used. However, numerous hazardous substances that are harmful to the environment and human health are regularly used in these procedures. Therefore, there is an increasing interest in biological approaches that do not involve the use of harmful chemicals or the formation of toxic byproducts. Among these, extracts prepared from plant leaves, seeds, roots, and stems are widely used in the production of green nanomaterials because they commonly contain polysaccharides, polyphenols, flavonoids, or alkaloids capable of functioning as agents of capping and reduction, facilitating the

[a]*Institute of Environmental Science, University of Rajshahi, Dr M A Wazed Miah Academic Building, Level # 1, Rajshahi-6205, Bangladesh*

[b]*Molecular Biology and Protein Science Laboratory, Department of Genetic Engineering and Biotechnology, University of Rajshahi, Sir Jagadish Chandra Bose Academic Building, Level # 4, Rajshahi-6205, Bangladesh. E-mail: reza.gen@ru.ac.bd*

[c]*Botany Division, Bangladesh Tea Research Institute, Sreemangal 3210, Moulvibazar, Bangladesh*

[d]*BCSIR Laboratories Rajshahi, Bangladesh Council of Scientific and Industrial Research (BCSIR), Rajshahi 6206, Bangladesh*

[e]*Bio & Nanotechnology Research Lab, Department of Materials Science and Engineering, University of Rajshahi, DrM A Wazed Miah Academic Building, Level # 3, Rajshahi-6205, Bangladesh*

[f]*Genetics and Molecular Biology Lab, Department of Zoology, University of Rajshahi, Sir Jagadish Chandra Bose Academic Building, Level # 2, Rajshahi-6205, Bangladesh*

† Electronic supplementary information (ESI) available. See DOI: https://doi.org/10.1039/d5na00115c

creation and preventing the agglomeration of nanoparticles. They are also usually harmless and biodegradable.[3,4]

Among the numerous types of metal-based nanoparticles, silver nanoparticles (AgNPs) have garnered significant interest over the years because of their distinctive physicochemical characteristics, which include chemical stability, good conductivity and antifungal, antiviral, antibacterial, and catalytic activities.[5] In recent years, the green synthesis of silver nanoparticles (AgNPs) has garnered noteworthy attention for its numerous advantages. Among the various biological methods, plant-based synthesis has emerged as a particularly promising approach that offers simplicity, scalability, and environmental sustainability. Plant extracts are rich in metabolites, *e.g.*, sugars, proteins, and various phytochemicals like terpenoids, polyphenols, alkaloids, and phenolic acids aid greatly in silver ion reduction (Ag^+) to metallic silver (Ag^0). The diverse and abundant phytochemicals present in these extracts not only act as reducing agents but also stabilize the nanoparticles, making plant-based synthesis a highly effective and eco-friendly alternative.[6–8] The tea plant, *Camellia sinensis* (L.) O. Kuntze has been a coveted source of non-alcoholic, caffeine-containing beverages since ancient times, with its origins tracing back to ancient China. Originally used as a medicinal drink, tea has evolved into a luxury beverage over the past 3000 years. Among the various tea varieties, green tea has gained considerable popularity in recent years because of its exceptional medicinal properties, including high antioxidant content. Green tea is known for its ability to promote intestinal health by supporting the propagation of beneficial microflora and safeguarding cellular and tissue systems from oxidative damage. Thus, green tea is an excellent oxygen-free radical scavenger. It also exhibits strong anti-inflammatory, antioxidant, and immune-boosting properties. From various notable epidemiological studies, the consumption of green tea can be further linked to a diminished risk of certain cancers, including those of the stomach, oral cavity, esophagus, and lungs.[9,10] In favor of its production process, green tea is notable for its high concentration of tea polyphenols and other antioxidant compounds, including gallic acid, epigallocatechin gallate, and other catechins.[11] Prior studies have emphasized the potential of green tea phytochemicals as highly effective reducing and stabilizing components in AgNP synthesis.[12–14] The hydroxyl groups (–OH) and carboxyl (–COOH) present in these polyphenols and other phytochemical compounds facilitate the reduction of Ag^+ ions, leading to AgNP synthesis.

In 1994, a remarkable breakthrough in nanoparticles was achieved with the advent of 'Oncaspar', a unique nanomedicine approved by the FDA for the treatment of Acute Lymphoblastic Leukemia by Servier Pharmaceuticals, followed by the approval of Doxil in 1995 by Janssen for the same indication. Since then, nanoparticles have gained importance in the development of anticancer drugs, enhancing the efficacy of existing chemotherapeutic agents, enabling targeted drug delivery, and overcoming drug resistance.[15–18] In recent years, green tea has gained attention for its health-promoting properties, which are largely attributed to green tea polyphenols (GTPs), namely catechin, epicatechin, epigallocatechin, epicatechin-3-gallate (ECG), and epigallocatechin-3-gallate (EGCG). Several studies have demonstrated the potential of GTPs to prevent carcinogenesis and suppress the proliferation of various malignant cells.[19–21]

In this study, AgNPs were synthesized using BT5 extract (green tea) as both a reducing and capping agent. A comprehensive characterization of the synthesized AgNPs was performed using a broad spectrum of techniques, including UV-vis spectroscopy to confirm nanoparticle formation, Dynamic Light Scattering (DLS) and zeta potential analysis to evaluate particle surface charge and size, Fourier-Transform Infrared Spectroscopy (FTIR) to identify functional groups associated with synthesis, Thermogravimetric Analysis (TGA) to evaluate thermal stability, X-ray Diffraction (XRD) to evaluate crystal structure evaluation, Field Emission Scanning Electron Microscopy (FE-SEM) and Energy Dispersive X-ray (EDX) to evaluate elemental and morphological composition. To explore potential biomedical applications, the anti-cancer activity of AgNPs was evaluated in a mouse model bearing Ehrlich-Lettre ascites carcinoma (EAC) cells. Further studies will investigate the impact of AgNPs on apoptosis-related gene expression, specifically analyzing the levels of p53, Bax, and Bcl2 in cancer cells.

Materials and methods

Materials

Dried leaves of BT5, a green tea cultivar (*Camellia sinensis* L. O. Kuntze), were procured from the Bangladesh Tea Research Institute (BTRI), Srimangal, Bangladesh, which is located at an altitude of 21.95 meters above the mean sea level. The remaining chemicals, *i.e.*, silver nitrate, ethanol, and methanol, were purchased from Sigma Aldrich, USA.

Phytochemical and antioxidant analysis of BT5 cultivar

The plant material was analyzed to determine its bioactive compounds and antioxidant properties. The Total Phenolic Content (TPC) of the BT5 ethanolic extract was quantified by employing the Folin–Ciocalteu method[22] with Gallic acid as the standard, while absorbance was recorded at 765 nm. A calibration curve (ESI, Fig. S1†) was generated using the equation $y = 0.0039x + 0.0318$ ($R^2 = 0.9986$). Using the aluminium chloride colorimetric assay,[23] the total flavonoid content (TFC) of the BT5 ethanolic extract was measured. Absorbance was detected at 415 nm using quercetin as the standard. The calibration curve was linear (ESI, Fig. S2†), with the equation $y = 0.0061x + 0.13$ ($R^2 = 0.9109$). The free radical scavenging property was investigated *via* 1,1-diphenyl-2-picrylhydrazyl radical (DPPH) assay[24] to quantify its ability to neutralize reactive oxygen species and calculated using the equation $\%RSA = ((Ac - As)/Ac) \times 100$. Using ascorbic acid as the standard, absorbance was recorded at 517 nm. The IC50 value, representing the concentration necessary to completely scavenge 50% of free radicals, was calculated from the linear regression equation $y = 0.0945x + 40.755$ ($R^2 = 0.8408$).

Further, specific phytochemical identification of the BT5 cultivar was performed *via* high-performance liquid chromatography (HPLC) (UltiMate 3000, DIONEX, Thermo SCIENTIFIC, Waltham, MA, USA) using a variable wavelength detector (VWD). As the non-polar stationary phase for HPLC, a C18 (Phenomenex, CA, USA) column was utilized (Particle size: 5 μm, pore size: 300 Å, dimension: 250 mm × 10 mm). Solvent A consisted of 0.1% trifluoroacetic acid (TFA) and 99.9% H_2O, whereas solvent B contained 100% acetonitrile and 0.1% TFA in the mobile phase. Data processing was performed using Chromeleon™ 6.8 software.

Preparation of the BT5 extracts

Dried BT5 leaves were pulverized, and 5 g of the resulting powder was boiled in deionized water (100 mL) at 60 °C for 30 minutes. After cooling, the concoction was passed through a filter paper (Whatman no. 1). A rotary evaporator (SENCO Technology Co., Ltd, Shanghai, China) was used for condensation of the collected filtrate and a vacuum oven for subsequent drying at 60 °C. The dried extract was ground using a mortar and pestle and stored in a freezer for future use as an agent to stabilize and reduce AgNP synthesis.

Green synthesis of BT5-AgNPs

A 450 mL solution of 5 mM silver nitrate ($AgNO_3$) was prepared in a beaker and placed on a hot plate magnetic stirrer (XMTD-702, China). Simultaneously, 50 mL of BT5 (green tea) extract was dissolved in deionized water (at 1 mg mL^{-1} concentration). Once the $AgNO_3$ solution reached 70 °C, the BT5 extract was gradually added to the beaker. The addition resulted in a notable color change from clear to brown, indicating that the silver ions were reduced to silver nanoparticles (Fig. 1). The mixture was stirred for an extended period of 20 minutes before being covered and stored in a dark place for 24 hours to stabilize the nanoparticles.

Centrifugation of the colloidal suspension was performed at 12 000 rpm at 4 °C for 20 minutes; the pellet obtained was washed thrice with ddH_2O and once with 100% ethyl alcohol using the centrifugation technique (Z36 HK, HERMLE Labortechnik GmbH, Wehingen, Germany). The purified nanoparticles were dispersed in deionized water (50 mL). A portion of the colloidal suspension was stored at 4 °C to assess its biological activity, whereas the rest of the suspension was vacuum-dried for biophysical characterization.

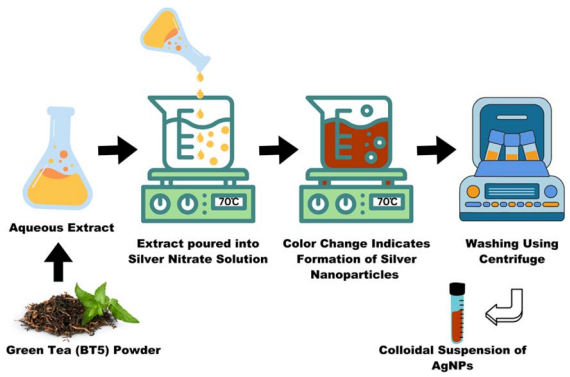

Fig. 1 Synthesis of AgNPs using green tea extract from BT5 cultivar. 5 mM $AgNO_3$ reduced using BT5 green tea extract and the color changes into dark brown indicating the formation of BT5-AgNPs.

Characterization of the synthesized BT5-AgNPs

UV-visible spectroscopy. The formation of BT5-AgNPs was confirmed by recording the UV-visible spectrum using a spectrophotometer (Genesys 150, Thermo Fisher Scientific, Waltham, Madison, USA). The precursor solution (5 mM $AgNO_3$) and the BT5 extract (1 mg mL^{-1}) were also analyzed. Spectral measurements were conducted in the wavelength range of 300–700 nm to identify the characteristic absorption peaks associated with the silver nanoparticles.

Dynamic light scattering (DLS). A particle size analyzer (Horiba analyzer, SZ-100, Kyoto, Japan) was used to determine the polydispersity index (PDI) along with the size distribution of the synthesized BT5-AgNPs. The colloidal dispersion was analyzed at 25 °C using DLS at a scattering angle of 90°. This method provided insights into the size and distribution of the nanoparticles.

Zeta potential. The zeta potentials of the synthesized BT5-AgNPs were measured using a Horiba SZ-100 analyzer (Kyoto, Japan). The analysis was performed to evaluate the stability of the colloidal nanoparticles in suspension and their surface charges.

Fourier-transform infrared (FTIR). Surface functional group identification of the synthesized AgNPs was completed using FTIR spectroscopy (PerkinElmer Spectrum 100, Shelton, CT, USA). FTIR spectra (4000–225 cm^{-1}) were recorded for both the BT5 extract and the BT5-AgNPs to identify functional groups involved in the synthesis. Background correction was achieved using a pure KBr pellet.

Thermogravimetric analysis (TGA). TGA was performed on both the BT5 extract and the synthesized BT5-AgNPs using a Simultaneous Thermal Analyzer (PerkinElmer STA 8000, Shelton, Connecticut, USA). The samples were heated at a controlled rate of 10 °C per minute under a nitrogen atmosphere. This inert nitrogen atmosphere prevented the oxidation of the samples during the heating process, ensuring that any observed weight loss was due to decomposition or volatilization of the sample components rather than oxidation reactions.

X-ray diffraction (XRD). The phases of the synthesized BT5-AgNPs and their crystalline structures were evaluated by XRD analysis using a Rigaku SmartLab® apparatus (Tokyo, Japan). The XRD pattern was obtained using Cu Kβ 1D radiation, scanning across a 2θ angle range of 5–80°. The analysis was conducted at an operating voltage of 40 kV and a current of 40 mA.

Field Emission Scanning Electron Microscope (FE-SEM) and Energy Dispersive X-ray (EDX). The morphology (size and shape) and elemental composition of the synthesized BT5-AgNPs were examined by FE-SEM (JSM-7610F, JEOL Ltd, Tokyo, Japan). This advanced imaging technique yielded high-resolution images of the nanoparticles, revealing their shape,

size distribution, and surface features. The FE-SEM also included an energy-dispersive X-ray spectroscopy (EDS) system, enabling the simultaneous analysis of the elemental composition, which provided insights into the presence of silver and any potential impurities.

In vivo experimental model and cell growth inhibition

A group of 24 male Swiss albino mice (8 weeks old, 25 ± 2 g) reared in the animal holding unit of the Molecular Biology and Protein Science Lab, Department of Genetic Engineering and Biotechnology, University of Rajshahi were used as *in vivo* experimental model animals. All mice were reared in cages maintained under ideal experimental conditions (25 °C ± 2 °C) with a 12 ± 1 hour dark/light cycle. Sufficient water and food (containing standard nutrients) were provided twice daily.

EAC cells were obtained from the Protein and Enzyme Laboratory, Department of Biochemistry and Molecular Biology, University of Rajshahi, Bangladesh.

With a slight modification, the previously reported methodology (Sur & Ganguly) was used to perform an *in vivo* EAC cell growth inhibition experiment. For the investigation, four mice groups ($n = 6$ for each group) were used. 5×10^6 EAC cells were injected intraperitoneally into each mouse. The treatments were initiated 24 hours after the injection of EAC cells and administered every day for five days. BT5-AgNPs were administered intraperitoneally to Groups 1 and 2 at doses of 1 mg kg^{-1} (low-concentration) and 5 mg kg^{-1} (high-concentration), respectively. Group 4 was the untreated control and was administered 0.9% NaCl, whereas bleomycin (0.5 mg kg^{-1}) was administered to Group 3. A 200 μL injection volume was used for all treatments and controls. On the sixth day after injecting EAC cells, the experimental subjects were euthanised, and the peritoneal fluid containing the cells was collected by washing the abdominal space with 1 mL of 0.9% salt solution. The collected cells were manually counted using a Neubauer haemocytometer (HBG, Germany) and a laboratory microscope (Optika, Italy). The efficacy of the treatments was assessed by calculating the inhibition of cell growth.

Ethical clearance

The Institutional Animal, Medical Ethics, Bio-safety and Bio-Security Committee (IAMEBBC) for Experimentation on Animal, Human, Microbes, and Living Natural Sources, memo no. 415 (27)/320/IAMEBBC/IBSc, Institute of Biological Sciences, University of Rajshahi, Bangladesh, granted permission to conduct this investigation.

Determination of EAC cell growth inhibition

Cell growth inhibition was calculated using the following formula previously described by Sur and Ganguly:[25]

$$\%\ \text{cell growth inhibition} = \left(1 - \frac{T_w}{C_w}\right) \times 100$$

where, T_w = mean number of EAC cells in the treated group. C_w = mean number of EAC cells in the control group of mice.

Assessment of apoptosis by DAPI staining

Morphological and nuclear alterations within EAC cells harvested from the control and treatment recipient sets of mice were examined using a fluorescence microscope (Olympus iX71, Hamburg, Germany). The extracted EAC cells (1 mL) were centrifuged at 4500 rpm (at 4 °C) for 5 minutes in a refrigerated centrifuge (Z36 HK, HERMLE Labortechnik GmbH, Wehingen, Germany). The resulting pellet was washed three times with normal saline (NS), with each wash at 4500 rpm (at 4 °C) for 2 minutes. The washed cells were subsequently stained using 5 μL of DAPI working solution (prepared from 10 mg mL^{-1} stock solution) for 15 minutes at 37 °C temperature in dark conditions, followed by a second centrifugation for 2 minutes at 4500 rpm. The DAPI-stained pellet was resuspended in 200 μL PBS. Finally, the cells were observed for morphological and nuclear alterations under a fluorescence microscope.

Gene expression analysis

The total RNA content of harvested EAC cells from the treated and placebo (control) groups was extracted using the Favor-Prep™ Total RNA Purification Mini kit (Favorgen, Ping Tung, Taiwan) following the instructions provided by the manufacturer. Nanodrop (Thermo Fisher, Madison, USA) was used for the quality assessment and quantification of RNA.

First-strand complementary DNA (cDNA) synthesis was performed using the TIANScript M-MLV (Tiangen^R, Beijing, China) protocol. Two steps were involved in the reaction. In 15 μL of total reaction volume, RNA was first combined with oligo(dT) primers and dNTPs (ESI, Table ST1†). The reaction mixture (3–5 μL) was then incubated in 20 μL of final reaction volume with M-MLV Reverse Transcriptase (RT) and 5× First-Strand Buffer (ESI, Table ST2†). The reaction mixture was electrophoresed using 1% agarose gel and stained with ethidium bromide to ensure the synthesis of cDNA.

Primers for the target genes (p53, BAX, BCl2) and the reference gene (GAPDH) were designed using Primer3 software, ensuring optimal length (18–30 nucleotides), melting temperature (T_m) between 50 °C and 60 °C and GC content (40–60%). The primers were cross-checked for specificity using an Oligo analyzer to avoid non-specific binding. The primer sequences are presented in Table 1.

Real-time polymerase chain reaction (RT-PCR) was conducted using GoTaq qPCR Master Mix (Promega Corporation, USA) on a qTower^3 G real-time PCR system (Analytik Jena,

Table 1 List of primers used in PCR and real-time PCR reaction

Primer name	Primer sequence
GAPDH-forward	5′-TCATCTCCGCCCCTTCTGC-3′
GAPDH-reverse	5′-TGCCTGCTTCACCACCTTCTT-3′
p53-forward	5′-GCGTCTTAGAGACAGTTGACT-3′
p53-reverse	5′-GGATAGGTCGGCGGTTCATCC-3′
BCl2-forward	5′-CAGCGGAGGAGGAGAAAGG-3′
BCl2-reverse	5′-GAATCGGGAGTTGGGGTCTG-3′
BAX-forward	5′-GCCCACCAGCTCTGAACAGATC-3′
BAX-reverse	5′-AAGTCCAGTGTCCAGCCCATG-3′

Germany). The reaction mixtures had a final volume of 20 μL, which contained 1 μL of cDNA template (10 times diluted), 10 μL of GoTaq qPCR Master Mix, 1 μL of forward primer (10 μM), 1 μL of reverse primer (10 μM), and 7 μL of nuclease-free water. A thermal cycler equipped with real-time detection was used for the amplification under the following conditions: initial denaturation for 3 minutes at 95 °C, 45 denaturation cycles for 15 seconds at 95 °C, annealing for 15 seconds at the primer-specific temperature, and extension for 20 seconds at 60 °C. The $2^{-(\Delta\Delta C_t)}$ method[26] was employed to calculate relative gene expression levels using Microsoft Excel.

Statistical analysis

A mean ± SD has been used to express the experimental results. To determine statistical significance, data were calculated using the ANOVA method in Microsoft Excel and GraphPad Prism 8. The *p*-value was required to be lower than 0.05 for a difference to be considered statistically significant. GraphPad Prism 8 and Origin2024b were used for the graphical presentation of data.

Result and discussion

Phytochemical and antioxidant properties of BT5 cultivar

The BT5 cultivar of green tea exhibited significant phytochemical and antioxidant properties, highlighting its potential as a viable nanoparticle synthesis agent. The BT5 extract had a TPC of 133.73 μg mL^{-1} (133.73 mg per g dry weight) and a TFC of 102.19 μg mL^{-1} (102.19 mg per g dry weight). The extract exhibited a concentration-dependent increase in antioxidant activity. At 12.5 μg mL^{-1}, the scavenging activity was 34.31%, which increased to 73.86% at 400 μg mL^{-1}. The estimated IC_{50} was approximately 97.8 μg mL^{-1}, suggesting moderate antioxidant activity (ESI, Fig. S3 and S4†). The HPLC analysis of the BT5 extract revealed significant peaks within the 9 to 12 minute retention time window, suggesting the presence of key polyphenolic compounds (Fig. 2). These peaks are linked to EGC and catechin, based on comparisons with recognized retention times.[27]

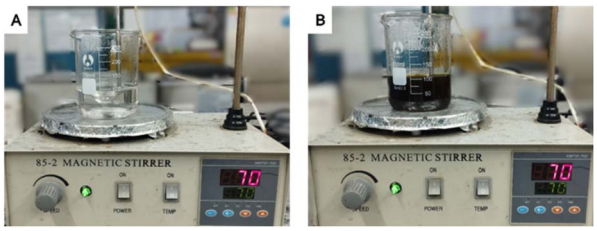

Fig. 3 Preparation of BT5-AgNPs. (A) Preheated $AgNO_3$ solution before adding BT5 extract and (B) drastic colour change into dark brown after adding BT5 water extract.

Preparation of BT5-AgNPs

The $AgNO_3$ solution was initially colorless, but upon gradual addition of the light brown BT5 green tea extract, the solution drastically turned dark brown, indicating the formation of colloidal AgNPs (Fig. 3). The compounds, which are mostly polyphenols present in the BT5 extract, help to form AgNPs from silver ions by donating electrons and acting as a stabilizing agent. Following visual confirmation, UV-vis, DLS, zeta, FT-IR, TGA, XRD, FE-SEM, and EDX were used to characterize BT5-AgNPS.[13]

Characterization of BT5-AgNPss

UV-visible spectroscopy analysis. A unique property of AgNPs is called localized surface plasmon resonance (LSPR). This means that they absorb light in the visible range, typically between 392 nm and 492 nm, creating a distinct peak.[28] The synthesized BT5-AgNPs were characterized using UV-vis spectroscopy to confirm their optical properties. The maximum absorbance (λ_{max}) was 424 nm (Fig. 4), confirming the formation of AgNPs. BT5 extract (blue line) and $AgNO_3$ solution (red line) do not show any significant absorbance, indicating that no AgNPs are present in the extract and that the Ag^+ ions have not yet reduced to AgNPs, respectively (Fig. 4). Previous studies reported that silver nanoparticles synthesized using green tea extracts exhibited UV-vis absorption peaks ranging from 400 to

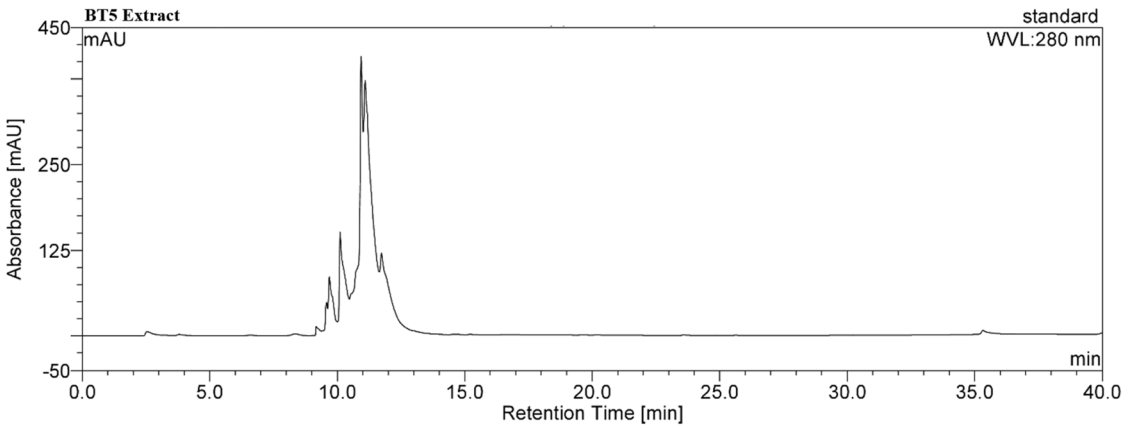

Fig. 2 HPLC chromatogram of methanolic leaf extract of BT5 tea genotype at 280 nm. The *x* axis denotes retention time and the *Y* axis denotes absorbance. Kromasil 100 C18 5μ 25 × 0.46 column was used to run the sample with water as solvent A and 80% acetonitrile as solvent B at 1 mL min^{-1} flow rate.

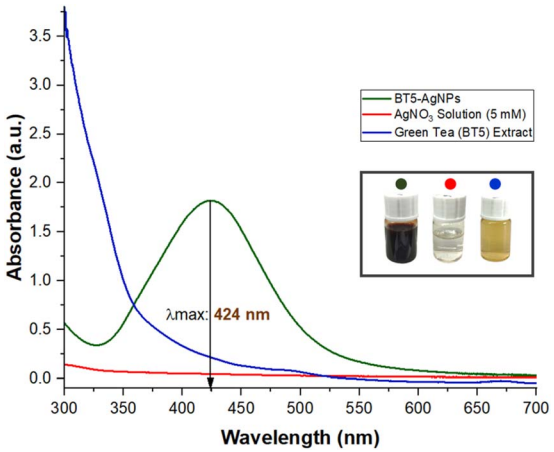

Fig. 4 Prominent peak between 400–500 nm on the UV-visible spectrum indicates BT5-AgNPs formation (green line) and compares with BT5 plant extract (blue line) and $AgNO_3$ solution (green line).

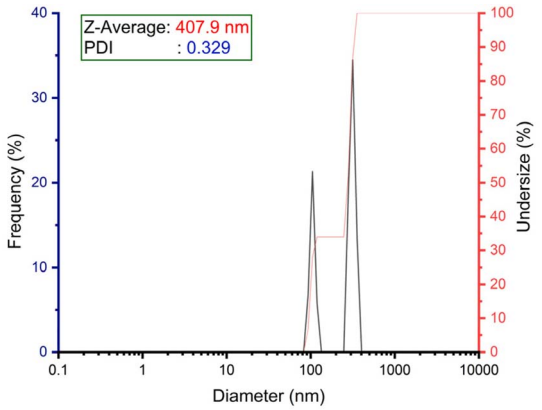

Fig. 5 DLS illustration shows a distribution of particle sizes, with the diameter on the *x*-axis and the frequency of that diameter on the *y*-axis.

490 nm, depending on particle size, shape, and synthesis conditions, as summarized in Table 2.

Dynamic light scattering (DLS). The DLS analysis revealed that the synthesized BT5-AgNPs exhibited a polydisperse size distribution (Fig. 5). The hydrodynamic diameter, or *Z*-average, was 407.9 nm (ESI, Table ST3†), greater than the size determined by FE-SEM (Fig. 10) because surface capping agents and solvation layers were present. The PDI of 0.329 indicates that the nanoparticles vary in size, implying that the sample has a generally uniform size distribution with acceptable quality for colloidal solutions (Fig. 5). Since a colloidal solution is considered "acceptable" if its PDI is less than 0.50, the BT5-AgNPs colloidal solution satisfies this requirement.[36,40]

Zeta potential. The colloidal stability of the amalgamate BT5-AgNPs was determined using zeta potential analysis, which resulted in a value of −39.8 ± 0.45 mV (Fig. 6). Commonly, nanoparticles with zeta potential values higher than ±30 mV are regarded as highly stable, whereas those between ±20 and ±30 are moderately stable.[32,36,37] The negative zeta potential (−39.8 ± 0.45 mV) observed in this study is attributed to the adsorption of negatively charged biomolecules (ESI, Table ST4†), most likely polyphenols (predominantly catechin)[12,32,41,42] from BT5 extract, which acts as agents of reduction and capping.

Fourier-transform infrared (FTIR). FTIR spectroscopy was used to confirm the formation of BT5-AgNPs and to identify the functional groups involved in the reduction and stabilization processes. The FTIR spectrum of the BT5 extract (red line in Fig. 7) exhibited several distinct peaks. A broad signal at 3251 cm^{-1} corresponds to O–H stretching vibrations, indicating that hydroxyl groups are generally detected in phenolic compounds. The peak at 2940 cm^{-1} is attributed to the C–H stretching vibrations of aliphatic compounds. Peaks at 1677 cm^{-1} and 1627 cm^{-1} represent the stretching vibrations of carbonyl (C=O) and alkene or aromatic (C=C) groups, respectively, which are characteristic of flavonoids and polyphenols present in the green tea extract. Additionally, peaks at 1224 cm^{-1}, 1125 cm^{-1}, and 1050 cm^{-1} correspond to the C–O stretching vibrations of ether (–C–O–C–) or alcohol (–C–OH) groups, while peaks at 1448 cm^{-1} and 1360 cm^{-1} are related to

Table 2 Absorbance characteristics of AgNPs synthesized from green tea extracts. The table summarizes previously reported data highlighting their λ_{max} value and associated FTIR absorption bands. The references of each data have been cited in the third column

λ_{max} (nm)	FT-IR peak frequencies (cm^{-1})	References
435	3440.90, 2362.488, 1641.11, 2085.86, 466.88	29
420	3439, 1630,1384	30
447	3280, 2912, 1630, 1533, 1373, 1248, 1016, 775	31
410	3440, 2913, 1630, 1392, 1044	32
424	3425.58, 2360.87, 1631.78, 1382.96, 1072.42, 829.39, 596	33
479	3434, 1630, 1021	34
470	3315, 1634	13
410	3689.8, 2924.09, 1634, 1238.9, 1701, 1043, 761.8	12
434	3333, 1634, 1403, 1247.9, 1058.3, 555.12	35
415	3411, 2916, 1743, 1107, 800, 406	36
263	3421.72, 2937.32, 2358.94, 1643.35, 1369.46, 1037.70	37
421	3455, 1638	38
420	3435, 2923, 1040, 825, 610	39

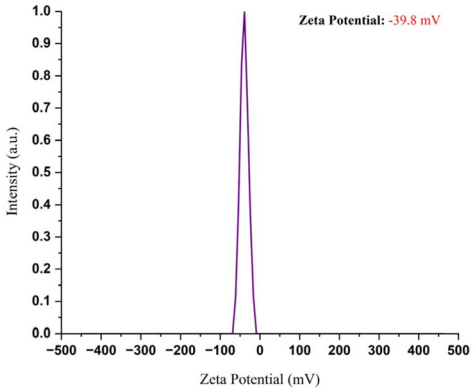

Fig. 6 Graph showing the zeta potential values of the synthesized BT5-AgNPs, indicating that the synthesized particles are highly stable and negatively charged.

the CH_2 and CH_3 bending vibrations of aliphatic compounds. These functional groups collectively confirm the bioactive molecules present in the BT5 extract and act as reducing and capping agents to convert Ag^+ ions to silver nanoparticles and stabilize them, thereby ensuring their colloidal stability.

The FTIR spectrum of the BT5-AgNPs (Fig. 7, blue line) revealed shifts in several key vibrational peaks compared with the BT5 extract (Fig. 7, red line), confirming the involvement of these functional groups in nanoparticle synthesis. The broad O–H stretching peak at 3251 cm^{-1} in the extract deviated to 3445 cm^{-1} in the BT5-AgNPs, consistent with the detected phenolic compounds and aromatic alcohols. Aliphatic C–H stretching was observed at 2932 cm^{-1}. Aromatic C=C stretching vibrations were evident at 1634 cm^{-1}. Further peaks at 1390 cm^{-1} and 1054 cm^{-1} were assigned to aromatic C–H bending and C–O stretching (ether linkage), respectively. The emergence of a new peak at 548 cm^{-1} is accredited to Ag–O stretching vibrations,[29,33,35,39] providing strong evidence for the interaction between the silver nanoparticles and the functional groups of the BT5 extract. These findings are consistent with previous reports on silver nanoparticle synthesis using green tea extract (Table 2).[12,13,29–39]

Thermogravimetric Analysis (TGA). TGA analysis of the BT5 extract (Fig. 8A) showed initial weight loss (<120 °C) due to moisture and volatile compounds, followed by significant weight loss (25.86% between 210–330 °C and 12.27% between 330–450 °C) attributed to the degradation of organic components (polyphenols, carbohydrates, proteins, lipids). The TGA of the BT5-AgNPs (Fig. 8B) demonstrated a slight initial weight loss (<200 °C) from moisture, followed by a gradual weight loss (33.57% between 200–720 °C), likely due to the combustion of organic aromatic compounds that might be capping or stabilizing the BT5-AgNPs. No further weight reduction was detected above 720 °C, indicating that the remaining 61.32% of particles were accredited to the presence of metallic silver. There was a considerable amount of organic material from the BT5 extract in the finished product, as the TGA data showed that the tea components in the synthesized BT5-AgNPs were responsible for about 39% of the weight reduction.[32,43]

X-ray diffraction (XRD). The XRD analysis confirmed the crystalline structure of the BT5-AgNPs. The XRD patterns of the

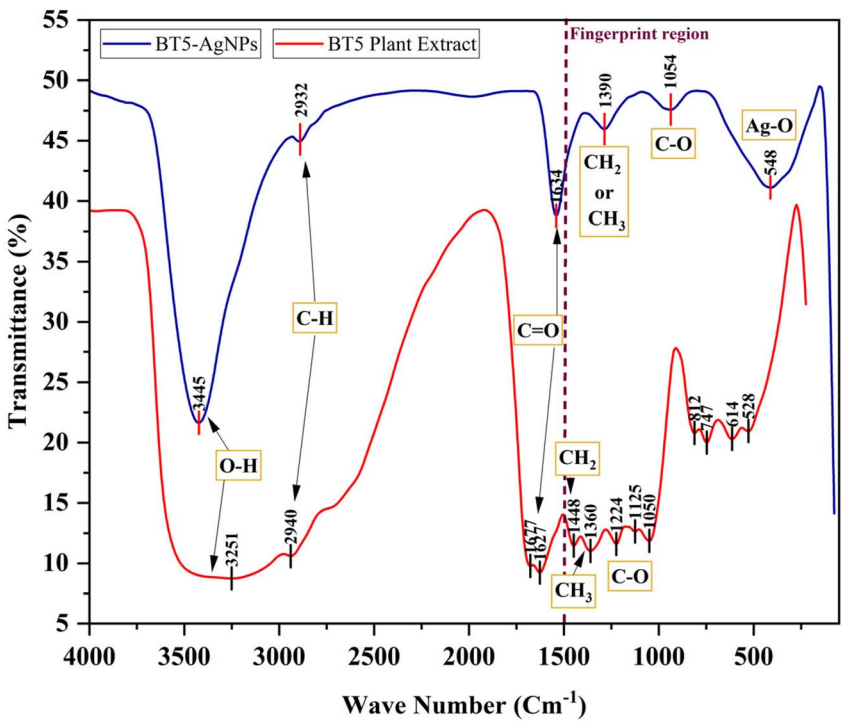

Fig. 7 Comparison of FT-IR spectra between BT5 plant extract (red line) and BT5-AgNPs (blue line) indicates the biomolecule present in the plant extract attached to the BT5-AgNPs surface during synthesis and causes the reduction of silver salt.

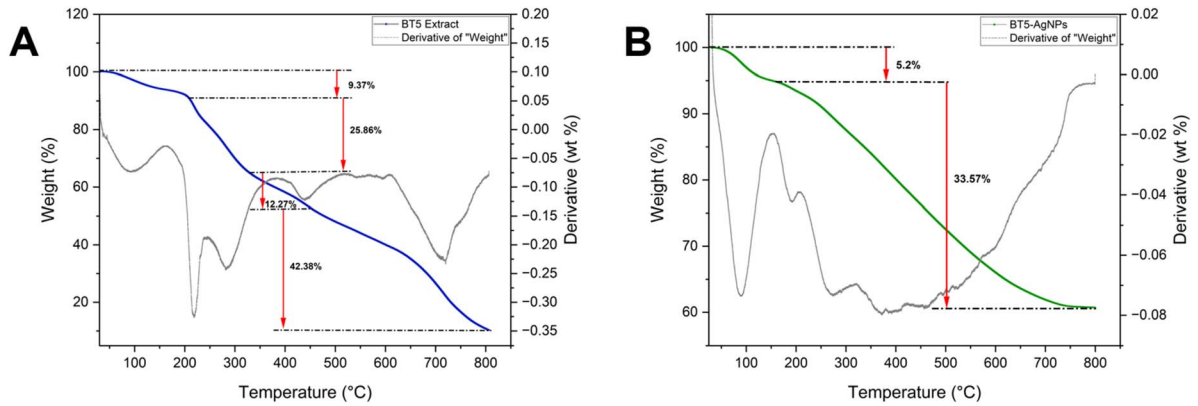

Fig. 8 Physical changes in BT5 green tea extract in response to different conditions. (A) TGA image showing the weight loss of BT5 green tea extract with temperature. (B) TGA image showing the weight loss of BT5-AgNPs with temperature.

dried BT5-AgNP samples (Fig. 9) revealed distinct peaks corresponding to the silver crystal lattice planes (111), (200), (220), and (311), confirming a face-centered cubic (FCC) crystal structure. These results indicate the formation of cubic-shaped, single-phase silver nanoparticles with no detectable presence of silver oxide (Ag_2O) or silver chloride (AgCl). This confirms the successful synthesis of pure AgNPs using BT5 green tea extract as a reducing and stabilizing agent and confirms prior research findings.[13,33,34,36,37] The average crystalline size (D) of the synthesized BT5-AgNPs was calculated using the Debye–Scherrer equation and was found to be 11.25 nm.

$$\text{Crystalline size}(D) = \frac{K\lambda}{\beta \cos\theta}$$

where K denotes the shape factor (0.9 for spherical particles), λ denotes the X-ray wavelength (0.1546 nm), while β denotes the full width at half maximum (FWHM) of the diffraction peak in radians, and θ is Bragg's angle. The crystalline sizes of all planes are given in Table 3.

Field Emission Scanning Electron Microscope (FE-SEM) and Energy Dispersive X-ray (EDX). The size, size distribution, shape, and elemental composition of the synthesized BT5-AgNPs were determined by FE-SEM examination. The morphology of the synthesized particles was studied, and the particle shape was mostly spherical; some were irregular, with an average size of 35 ± 8.36 nm (Fig. 10). The weight percentages (W%) of silver, carbon, nitrogen, and oxygen were 61.44, 13.27, 7.71, and 17.58, respectively (Fig. 11). The high

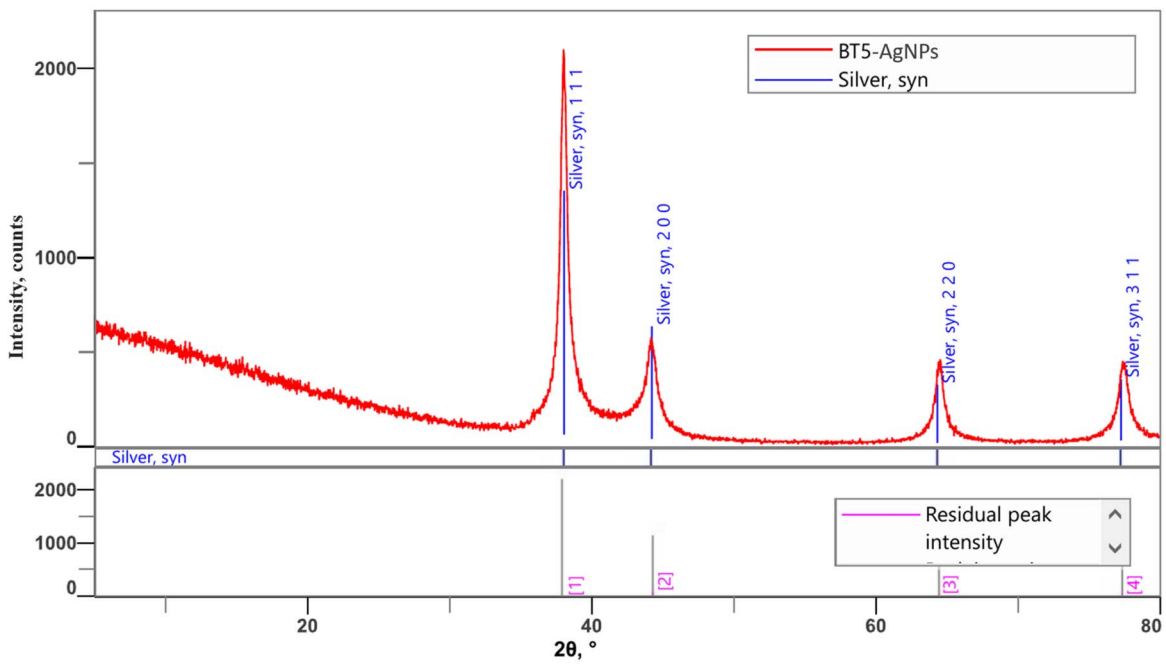

Fig. 9 XRD peak of BT5-AgNPs corresponding to the silver lattice planes (111), (200), (220) and (311), indicating that the synthesized particles are cubic-shaped, single-phase BT5-AgNPs.

Table 3 Crystalline sizes of planes

Sl. no.	Planes (*hkl*)	2θ	Sin(θ)	Cos(θ)	FWHM (β) radians	Inter-planar spacing (d)	Lattice constant (a)	Cell volume (a^3)	Crystalline size (D) (nm)
1	111	37.94733	0.325134	0.945668	0.011402	2.36917	4.103523	69.098808	12.86
2	200	44.25451	0.376665	0.92635	0.023651	2.04504	4.09008	68.421944	6.33
3	220	64.34297	0.532455	0.846458	0.013251	1.44669	4.091857	68.511175	12.36
4	311	77.27808	0.624412	0.781095	0.013207	1.23364	4.091521	68.494288	13.44

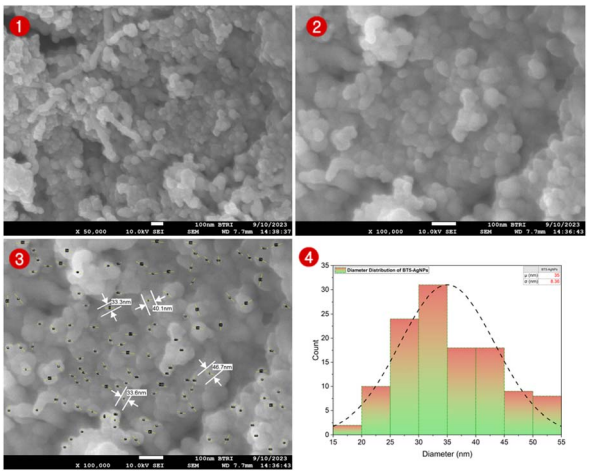

Fig. 10 SEM images of BT5-AgNPs. (A) At 50 000 magnifications, (B) at 100 000 magnifications, (C) determination of particle size using Image J software, and (D) corresponding size distribution histograms of BT5-AgNPs.

abundance of silver (61.44%) confirms the presence of silver nanoparticles in the sample, consistent with the observations of the TGA thermographs. The presence of carbon, nitrogen, and oxygen suggests the presence of organic molecules in the BT5 extract, which is used as a reduction and capping agent. The absorption peak for Pt can be attributed to the platinum-coating used in sample preparation before SEM/EDX analysis.

Anti-proliferative activity of synthesized BT5-AgNPs on EAC cells

Based on these findings, the antiproliferative activity of BT5-AgNPs was determined. The synthesized BT5-AgNPs were subjected to experimentation to determine their capacity to reduce cancer cell proliferation using EAC cells induced in Swiss albino mice as a cancer model. Following six days of therapy, both the low-concentration dosage (1 mg kg^{-1} of body weight per day) and high-concentration dosage (5 mg kg^{-1} of body weight per day) treatment groups inhibited EAC cell development, with the low dose showing significant outcomes. The concentrations (1 mg kg^{-1} and 5 mg kg^{-1} body weight per day) reported for BT5-AgNPs represent the concentration of the entire nanoparticle formulation (*i.e.*, the total weight of nanoparticles). Specifically, the low-dose group achieved 52.15% inhibition of cancer cell proliferation compared with 22.91% inhibition observed in the high-dose group (Fig. 12). The chemotherapeutic drug bleomycin was deliberately selected as a positive

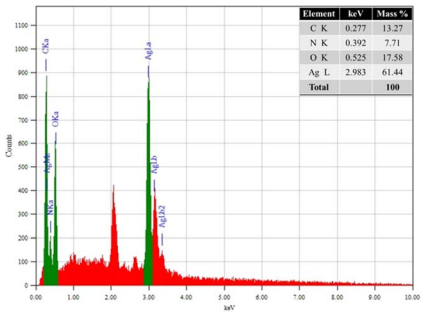

Fig. 11 EDX spectra showing the elemental compositions of the synthesized BT5-AgNPs.

control at a standard therapeutic dosage of 0.5 mg kg^{-1} body weight per day based on established literature and clinical usage guidelines. Although this dosage differs from the nanoparticle concentrations tested, bleomycin's purpose was solely to serve as a validated reference point for its effective antiproliferative activity.[44] The standard drug exhibited 81.59% suppression of EAC cell growth. The reduced efficacy observed at higher BT5-AgNP concentrations may be attributed to cytotoxic effects or altered cellular responses, highlighting the need for further optimization.

Our findings align with earlier research, which demonstrated the anticancer efficacy of green tea extract-mediated AgNPs against EAC cells *in vivo* and enhanced therapeutic potential with minimum toxicity.[45,46] Many other studies have highlighted the broad-spectrum chemotherapeutic activity of green tea-mediated AgNPs against MCF-7, HeLa, Hep-2, A549, KB3, AGS, and NTERA-2.[31,47,48]

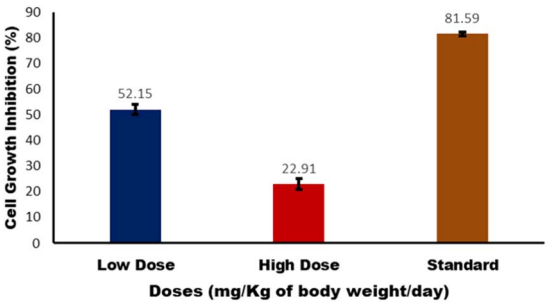

Fig. 12 Bar chart illustrating cell growth inhibition (%) of EAC cells at different dosages (mg kg^{-1} of body weight per day). The standard dosage (bleomycin) shows the highest inhibition, followed by the low-concentration dosage. The high-concentration dosage exhibits the lowest inhibition. The error bars represent the standard deviation.

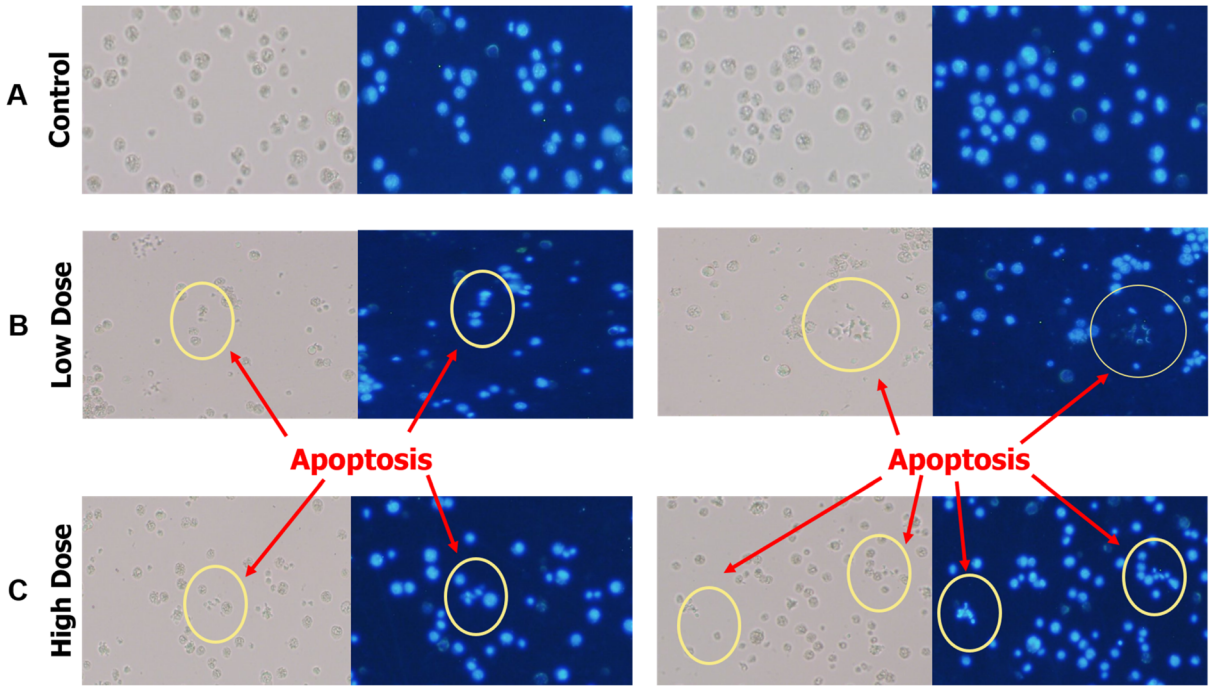

Fig. 13 (A) Fluorescence microscopic view of the control shows that the cells are intact and have no signs of apoptosis, (B) fluorescence microscopic view of EAC cells for low-dose treated mice displayed that the cells are going through apoptosis, and (C) fluorescence microscopic view of EAC cells for high-dose treated mice displayed that the cells are going through apoptosis.

Detection of apoptosis EAC cell by DAPI staining

To further investigate the mechanism underlying the anti-proliferative activity of BT5-AgNPs, DAPI staining was employed to determine whether EAC cells are undergoing apoptotic transformation or not. Fluorescence microscopy revealed notable differences between untreated control and treated cells. The control cells had a normal, rounded appearance with homogeneous nuclear staining (Fig. 13A). Cells treated with BT5-AgNPs (low-dose group and high-dose group) exhibited apoptotic characteristics such as heterochromatization, Karyorrhexis, bleb formation on the membrane, and shrinkage of cells (Fig. 13B and C). These structural alterations represent signs of apoptosis, a process of controlled cell death that rids the body of undesired or damaged cells while sparing healthy tissue.

Expression of p53, BAX and Bcl2 gene analysis

The total RNA content extracted from the recipient EAC cells of treatment and placebo showed high purity and integrity (ESI,

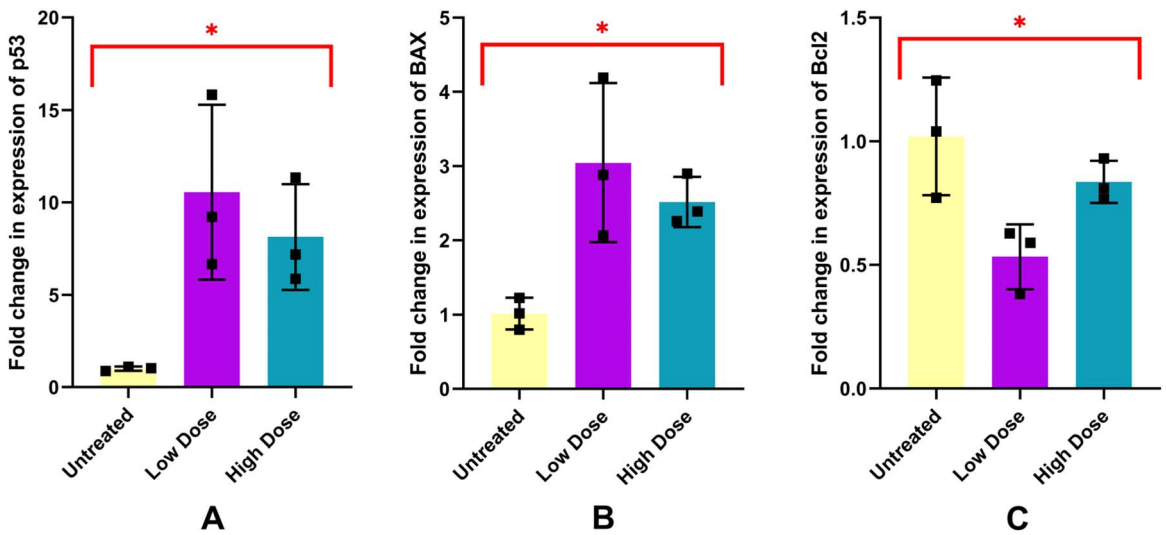

Fig. 14 Bar chart showing a fold change in the expression of p53 (A), BAX (B), and Bcl2 (C) in EAC cells with low and high doses of BT5-AgNPs treatment compared to an untreated group. Error bars represent the standard deviation. (*) indicate statistically significant differences compared to the untreated group ($p < 0.05$).

Fig. S5 and Table ST5†). cDNA synthesis (ESI, Table ST6†) and RT-qPCR were conducted according to the protocol presented in the methodology. The $2^{-(\Delta\Delta C_t)}$ method[26] was used to quantify relative gene expression by normalizing data to a reference gene (GAPDH in this study).

The gene expression analysis revealed a dose-dependent modulation of the apoptotic pathway. p53 expression was upregulated 10 times in the low-dosage recipient group and 8 times in the high-dosage recipient group, suggesting activation of the intrinsic apoptotic pathway. Similarly, BAX, a pro-apoptotic gene, was upregulated 3 times in the low-dosage recipient group and 2.5 times in the high-dosage recipient group, thereby enhancing pro-apoptotic signalling. The anti-apoptotic gene BCl2 was downregulated 0.53 times in the low-dosage recipient group and 0.84 times in the high-dosage recipient group, reflecting reduced anti-apoptotic defences (Fig. 14). These results demonstrate that low-dose therapy promotes apoptosis better than high-dose therapy through the upregulation of p53 and BAX and downregulation of BCl2. This supports the notion of dose-dependent effects of nanoparticles in cancer therapy, as observed in previous studies.[47]

Conclusion

This study used BT5 extract, a commercial green tea cultivar from Bangladesh, to synthesize silver nanoparticles (BT5-AgNPs) using an eco-friendly, green approach. Before synthesis, the BT5 extract was analysed, revealing significant amounts of bioactive compounds, such as total phenolics, flavonoids, and demonstrating strong antioxidant activity. These bioactive components are believed to contribute to the reduction and stabilization of silver ions during synthesis. The synthesized BT5-AgNPs were characterized using FE-SEM, EDX, XRD, FTIR, UV-vis spectroscopy, DLS, zeta potential, and TGA techniques to confirm their size, elemental composition, crystalline structure, PDI, hydrodynamic diameter, and surface charge. The FT-IR results indicated that the green-synthesized BT5-AgNPs displayed similar diffraction peaks and chemical functional groups as the BT5 extract, suggesting the involvement of phytochemicals in reducing Ag^+ to AgNPs. Furthermore, BT5-AgNPs exhibit enhanced thermal stability compared with green tea extract. The antiproliferative activity of the synthesized BT5-AgNPs was assessed in an experimental tumor model. The results demonstrate significant inhibition of cell growth and apoptosis-inducing ability. Expression analysis revealed a dose-dependent modulation of key apoptotic genes, including downregulation of BCl2 and upregulation of p53 and BAX, further supporting their potential as natural therapeutic agents for cancer treatment.

Data availability

The data supporting the findings of this article are included in the ESI.†

Author contributions

Sk. Md. Atiqur Rahman: methodology, investigation, formal analysis, writing–original draft, writing–review & editing, visualization, project administration, and data curation. Rokshana Ara Ruhi: methodology, investigation, writing–original draft, and writing–review & editing. Md. Mahmudul Hasan Maruf: investigation. Md. Ragib Shariar: investigation. Mobasshir Noor Shehab: investigation and writing–review & editing. Khaled Mahmud Sujon: investigation. Mohammad Saiful Islam: investigation. Md. Abdul Aziz: investigation. Firoz Ahmed: investigation. Ananda Kumar Saha: writing–review & editing. Md. Anwarul Kabir Bhuiya: writing–review & editing, supervision, and funding acquisition. Md. Abu Reza: conceptualization, supervision, resources, writing–review & editing, validation, and funding acquisition.

Conflicts of interest

The authors declare that there are no conflicts of interest.

Acknowledgements

The current research was supported by a special research grant of Rajshahi University (A-701/6/109 (research), 2022) and the Ministry of Education's Grant for Advanced Research in Education (GARE) (Project ID: PS20201507 and ET20232558). The authors wish to extend their sincere gratitude to the Bangladesh Council of Scientific and Industrial Research for their support with DLS, Zetasizer, and FE-SEM with EDX instruments. Additionally, we acknowledge the Molecular Pathology Laboratory, Institute of Biological Science, R. U., and the Plant Breeding and Gene Engineering Lab, Department of Botany, R.U. for their assistance with HPLC and phytochemical analysis.

References

1 M. Xing, L. Ge, M. Wang, Q. Li, X. Li and J. Ouyang, *Int. J. Nanomed.*, 2014, 2399, DOI: 10.2147/ijn.s55015.
2 H. Chen, M. C. Roco, X. Li and Y. Lin, *Nat. Nanotechnol.*, 2008, **3**, 123–125.
3 M. Govarthanan, Y.-S. Seo, K.-J. Lee, I.-B. Jung, H.-J. Ju, J. S. Kim, M. Cho, S. Kamala-Kannan and B.-T. Oh, *Artif. Cells, Nanomed., Biotechnol.*, 2016, **44**, 1878–1882.
4 O. V. Kharissova, H. V. R. Dias, B. I. Kharisov, B. O. Pérez and V. M. J. Pérez, *Trends Biotechnol.*, 2013, **31**, 240–248.
5 M. Baghayeri, B. Mahdavi, Z. Hosseinpor-Mohsen Abadi and S. Farhadi, *Appl. Organomet. Chem.*, 2018, **32**, 2.
6 K.-J. Lee, S.-H. Park, M. Govarthanan, P.-H. Hwang, Y.-S. Seo, M. Cho, W.-H. Lee, J.-Y. Lee, S. Kamala-Kannan and B.-T. Oh, *Mater. Lett.*, 2013, **105**, 128–131.
7 V. V. Makarov, A. J. Love, O. V. Sinitsyna, S. S. Makarova, I. V. Yaminsky, M. E. Taliansky and N. O. Kalinina, *Acta Naturae*, 2014, **6**, 35–44.
8 K. Parveen, V. Banse and L. Ledwani, *AIP Conf. Proc.*, 2016, **1724**, 1.
9 A. Rietveld and S. Wiseman, *J. Nutr.*, 2003, **133**, 3285S–3292S.
10 T. Kondo, T. Ohta, K. Igura, Y. Hara and K. Kaji, *Cancer Lett.*, 2002, **180**, 139–144.

11 S. Wang, N. Moustaid-Moussa, L. Chen, H. Mo, A. Shastri, R. Su, P. Bapat, I. Kwun and C.-L. Shen, *J. Nutr. Biochem.*, 2014, **25**, 1–18.
12 H. A. Widatalla, L. F. Yassin, A. A. Alrasheid, S. A. Rahman Ahmed, M. O. Widdatallah, S. H. Eltilib and A. A. Mohamed, *Nanoscale Adv.*, 2022, **4**, 911–915.
13 K. Parvathalu, D. N. Kumar, K. Rajitha, M. G. Kishan, B. N. Kumar, J. Bhemarajam, S. R. Naidu, G. L. Merlinsheeba, P. Mandal, S. Banne, A. Dayanand, V. Morampudi, B. Murali, S. E. N. Vinodini, Y. V. Reddy and P. B. Bhaskar, *Plasmonics*, 2023, **18**, 1837–1845.
14 M. Golpour, P. Ebrahimnejad, Z. R. Gatabi, A. Najafi, A. Davoodi, R. Khajavi, M. Alimohammadi and T. Mousavi, *Inorg. Chem. Commun.*, 2024, **161**, 111989.
15 M. J. Mitchell, M. M. Billingsley, R. M. Haley, M. E. Wechsler, N. A. Peppas and R. Langer, *Nat. Rev. Drug Discovery*, 2021, **20**, 101–124.
16 H. Sabit, M. Abdel-Hakeem, T. Shoala, S. Abdel-Ghany, M. M. Abdel-Latif, J. Almulhim and M. Mansy, *Pharmaceutics*, 2022, **14**, 1566.
17 A. Rodzinski, R. Guduru, P. Liang, A. Hadjikhani, T. Stewart, E. Stimphil, C. Runowicz, R. Cote, N. Altman, R. Datar and S. Khizroev, *Sci. Rep.*, 2016, **6**, 20867.
18 M. M. Safhi, S. M. Sivakumar, A. Jabeen, F. Zakir, F. Islam, T. Anwer, U. S. Bagul, M. E. Elmobark, G. Khan, R. Siddiqui, A. Hussien and M. F. Alam, *Elsevier*, 2017, 159–169, DOI: 10.1016/b978-0-323-52725-5.00008-3.
19 C. S. Yang, X. Wang, G. Lu and S. C. Picinich, *Nat. Rev. Cancer*, 2009, **9**, 429–439.
20 A. Bag and N. Bag, *J. Nat. Sci. Biol. Med.*, 2018, **9**, 2.
21 Y. Miyata, T. Matsuo, K. Araki, Y. Nakamura, Y. Sagara, K. Ohba and H. Sakai, *Medicines*, 2018, **5**, 87.
22 M. Nasiruddin and S. N. Sinha, *Asian J. Med. Biol. Res.*, 2020, **6**, 187–195.
23 C. Quettier-Deleu, B. Gressier, J. Vasseur, T. Dine, C. Brunet, M. Luyckx, M. Cazin, J.-C. Cazin, F. Bailleul and F. Trotin, *J. Ethnopharmacol.*, 2000, **72**, 35–42.
24 İ. Gulcin and S. H. Alwasel, *Processes*, 2023, **11**, 2248.
25 P. Sur and D. Ganguly, *Planta Med.*, 1994, **60**, 106–109.
26 K. J. Livak and T. D. Schmittgen, *Methods*, 2001, **25**, 402–408.
27 P. L. Fernandez, M. J. Martin, A. G. Gonzalez and F. Pablos, *Analyst*, 2000, **125**, 421–425.
28 D. Paramelle, A. Sadovoy, S. Gorelik, P. Free, J. Hobley and D. G. Fernig, *Analyst*, 2014, **139**, 4855.
29 A. Kharabi Masooleh, A. Ahmadikhah and A. Saidi, *IET Nanobiotechnol.*, 2019, **13**, 183–188.
30 W. Xu, Y. Fan, X. Liu, D. Luo, H. Liu and N. Yang, *Mater. Res. Express*, 2018, **5**, 045029.
31 D. Arumai Selvan, D. Mahendiran, R. Senthil Kumar and A. Kalilur Rahiman, *J. Photochem. Photobiol., B*, 2018, **180**, 243–252.
32 W. R. Rolim, M. T. Pelegrino, B. De Araújo Lima, L. S. Ferraz, F. N. Costa, J. S. Bernardes, T. Rodigues, M. Brocchi and A. B. Seabra, *Appl. Surf. Sci.*, 2019, **463**, 66–74.
33 P. Prema, V. Veeramanikandan, K. Rameshkumar, M. K. Gatasheh, A. A. Hatamleh, R. Balasubramani and P. Balaji, *Environ. Res.*, 2022, **204**, 111915.
34 Y. Fang, C.-Q. Hong, F.-R. Chen, F.-Z. Gui, Y.-X. You, X. Guan and X.-H. Pan, *Inorg. Chem. Commun.*, 2021, **132**, 108808.
35 A. Bergal, G. H. Matar and M. Andaç, *BioNanoScience*, 2022, **12**, 307–321.
36 M. A. Taleb Safa and H. Koohestani, *Results Eng.*, 2024, **21**, 101808.
37 H. H. Salih, *Baghdad Sci. J.*, 2024, **21**, 1470.
38 D. Hermanto, N. Ismillayli, D. H. Fatwa, U. K. Zuryati, H. Muliasari, R. Wirawan, D. Prasetyoko and S. Suprapto, *S. Afr. J. Chem. Eng.*, 2024, **47**, 136–141.
39 A. Wirwis and Z. Sadowski, *ACS Omega*, 2023, **8**, 30532–30549.
40 P. Mukhopadhyay and P. P. Kundu, *RSC Adv.*, 2015, **5**, 93995–94007.
41 M. Singh, A. Mallick, M. Banerjee and R. Kumar, *Bull. Mater. Sci.*, 2016, **39**, 1871–1878.
42 M. Flores-González, M. Talavera-Rojas, E. Soriano-Vargas and V. Rodríguez-González, *New J. Chem.*, 2018, **42**, 2133–2139.
43 Q. Sun, X. Cai, J. Li, M. Zheng, Z. Chen and C.-P. Yu, *Colloids Surf., A*, 2014, **444**, 226–231.
44 *Pfizer, bleomycin for Injection*, USP, https://www.pfizermedicalinformation.com/patient/bleomycin.
45 M. E. Hosen, M. A. Rahman, M. S. Rahman, S. Akash, M. Khalekuzzaman, A. A. Alsahli, M. Bourhia, H. A. Nafidi, M. A. Islam and R. Zaman, *Chem. Biodiversity*, 2024, **21**, 3.
46 A. Magdy, E. Sadaka, N. Hanafy, M. A. El-Magd, N. Allahloubi and M. El Kemary, *Mol. Cell. Toxicol.*, 2020, **16**, 271–282.
47 F. Mobaraki, M. Momeni, M. Jahromi, F. M. Kasmaie, M. Barghbani, M. E. T. Yazdi, Z. Meshkat, F. H. Shandiz and S. M. Hosseini, *Process Biochem.*, 2022, **119**, 106–118.
48 S. K. Sahu, A. Mansoori, S. K. Jana, A. Kumar and T. K. Ghorai, *J. Mol. Struct.*, 2025, **1320**, 139690.